ISTS 2006-k-09

TERRAMECHANICS-BASED ANALYSIS ON SLOPE TRAVERSABILITY FOR A PLANETARY EXPLORATION ROVER

Genya Ishigami, Akiko Miwa, Keiji Nagatani and Kazuya Yoshida
Department of Aerospace Engineering, Tohoku University
Aoba 6-6-01, Sendai, 980-8579, JAPAN
(E-mail : ishigami@astro.mech.tohoku.ac.jp)

Abstract

In this paper, the slope traversability analysis for a planetary exploration rover based on a terramechanics approach is described. In this research, the slope traversability is defined as consisting of both slope climbing and traversing (crossing) capabilities. The authors have investigated traction mechanics between a wheel of a rover and loose soil. Applying our previous works in the wheel-soil interactions to the slope traversability of the rover, two criteria dominating the slope traversability named as "Mobility limit" and "Trafficability limit" are investigated. The mobility limit is determined by a margin between the torque limit of a wheel driving motor and the resistance torque to the wheel. The trafficability limit is also determined by relationship between the traction load of the rover and the summation of traction forces generated by wheels. Through a number of slope climbing/traversing experiments using our rover test bed, the slope traversability of the rover is analyzed by the proposed criteria.

1. Introduction

An investigation of internal materials of a planetary body is an important mission to better understand the origin of the planetary body. It is known that exploration into a crater is one effective approach to investigate internal materials of a planet, since a central peak in the crater (diameter $\geq$ 35 [km]) emerged due to the impact of a large meteorite can consists of materials found only at depth of 10 [km] of the planetary body [1].

A planetary rover is one key technology to explore inside a crater. The rover has to have enough capabilities to travel highly challenging terrains, climb or traverse slopes of the crater. However, the planetary surface terrain including craters, such as on the Moon or Mars, is mostly covered with fine-grain loose soil called regolith. Dealing with slopes around the crater is then a difficult task since the wheels of the rover might easily slip or loose their traction on such sandy soil. In addition, those slips will increase when the rover climbs or traverses the slope. It is deduced that slopes climbing/traversing capabilities (the slope traversability) of the rover will be dominated by dynamic interactions between wheels and the regolith.

The research field regarding the wheel-soil interaction has been investigated in a field called "Terramechanics." For instance, analysis of wheel-soil interaction mechanism and modelling of stress distributions underneath a wheel have been well studied in [2-4]. Iagnemma et al. have applied those terramechanics models to traction mechanics of planetary rovers [5,6]. We have elaborated a wheel-and-vehicle dynamics model, which is able to deal with motion characteristics of planetary rovers [7,8]. The slope climbing capability of a rover has also been discussed in [7], but detailed criteria to determine the slope traversability of a rover are still left as an open issue.

In this paper, the slope traversability analysis based on a terramechanics approach is addressed applying our background in regard to the dynamic interaction of a wheel on loose soil [7,8]. The wheel-soil contact model developed in [8] has to be improved to deal with a wheel on an inclined surface. Also, to clarify the characteristics of the wheel's forces/torque (a drawbar pull, a side force and a resistance torque), we have carried out single wheel experiments and numerical simulations.

Then, the slope traversability criteria are proposed through discussing the characteristics of the wheel forces and torque. One of the criteria is named "mobility limit" and the other is "trafficability limit." The mobility limit is simply caused by relationship between the torque limit of a wheel driving motor and the resistance torque to the wheel. On the other hand, the trafficability limit is determined by the traction load of a rover and the summation of the wheels' forces (drawbar pulls and side forces.)

Additionally, the slope climbing/traversing experiments using our rover test bed are carried out in order to analyze the slope traversability of the rover. According to those slope experiments, it is found that the proposed criteria are able to analyze the slope traversability of the rover.

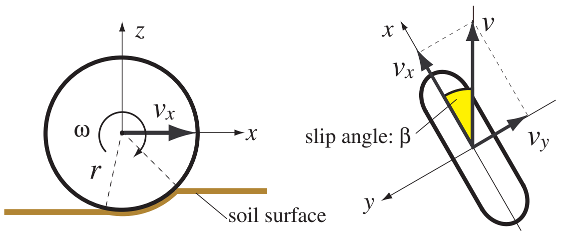

Fig. 1: Wheel coordinate system

2. Wheel-Soil Contact Model

The following analysis deals with a rigid wheel which rotates on loose soil. A wheel coordinate system is defined using right-hand frame as shown in Fig. 1, where the longitudinal direction is denoted by x, the lateral direction by y, and the vertical direction by z. The coordinate frame turns according to a steering action of the wheel (the yaw rotation around the z axis) but does not rotate with a driving motion of the wheel (the pitch rotation around the y axis).

2.1 Slip ratio and slip angle

When a wheel travels on loose soil, the wheel slips both in the longitudinal and lateral directions, respectively. The slip in the longitudinal direction is measured by "slip ratio," which is defined as a function of the longitudinal traveling velocity v_x and the circumference velocity of the wheel $r\omega$:

$$s = \begin{cases} (r\omega - v_x)/r\omega & (r\omega > v_x : \text{driving}) \\ (r\omega - v_x)/v_x & (r\omega < v_x : \text{braking}) \end{cases} \tag{1}$$

The slip ratio takes a value between -1 and 1.

On the other hand, the slip in the lateral direction is measured by "slip angle," which is defined by the longitudinal and lateral traveling velocities v_y of the wheel as follows:

$$\beta = \tan^{-1}(v_y/v_x) \tag{2}$$

2.2 Normal stress and shear stress

To deal with the normal and shear stress of a wheel is indispensable to obtain wheel forces. Based on terramechanics models, the stress under the wheel can be modeled as shown in Fig. 2-(a).

The normal stress $\sigma(\theta)$ is described according to [8]:

$$\sigma(\theta) = \begin{cases} \sigma_m \left(\dfrac{\cos\theta - \cos\theta_f}{\cos\theta_m - \cos\theta_f} \right)^n & (\theta_m \le \theta < \theta_f) \\ \sigma_m \left(\dfrac{\cos\{\theta_f - \frac{\theta - \theta_r}{\theta_m - \theta_r}(\theta_f - \theta_m)\} - \cos\theta_f}{\cos\theta_m - \cos\theta_f} \right)^n & \\ & (\theta_r < \theta \le \theta_m) \end{cases} \tag{3}$$

θ_m is the specific wheel angle at which the normal stress is maximized [9]. The maximum stress σ_m is defined by the following equation [4]:

$$\sigma_m = r^n (k_c/b + k_\phi)(\cos\theta_m - \cos\theta_f)^n \tag{4}$$

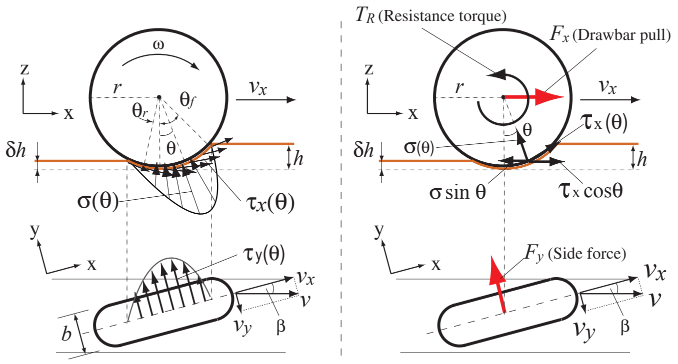

(a) : Stress model (b) : Force model

Fig. 2: Wheel-soil contact model

where k_c, k_ϕ and n are the soil-specific parameters. b is the width of the wheel.

The shear stresses $\tau_x(\theta)$ and $\tau_y(\theta)$ are written by the same expressions:

$$\tau_i(\theta) = (c + \sigma(\theta)\tan\phi)[1 - e^{-j_i(\theta)/k_i}], \quad (i = x, y) \tag{5}$$

The symbols used in the equation (5) are listed as follows:

- c : cohesion stress of soil
- ϕ : internal friction angle of soil
- j_i : soil deformation in each direction
- k_i : shear deformation module in each direction

2.3 Drawbar pull : F_x

A general force model for a rigid wheel on loose soil is presented in Fig. 2-(b). Using the normal stress $\sigma(\theta)$ and the shear stress in x direction $\tau_x(\theta)$, Drawbar pull F_x that exerts from the soil to the wheel is calculated by the integral from an entry angle θ_f to an exit angle θ_r [3]:

$$F_x = rb \int_{\theta_r}^{\theta_f} \{\tau_x(\theta)\cos\theta - \sigma(\theta)\sin\theta\} d\theta \tag{6}$$

2.4 Side force : F_y

Side force F_y appears at the lateral direction of the wheel when the wheel or the vehicle makes steering. The current authors have modeled the side force as follows [8]:

$$F_y = \int_{\theta_r}^{\theta_f} \{rb \cdot \tau_y(\theta) + R_b \cdot (r - h(\theta)\cos\theta)\} d\theta \tag{7}$$

R_b is the reaction resistance generated by the bulldozing phenomenon on the side face of the wheel. R_b is given as a function of a wheel sinkage h.

2.5 Resistance torque : T_R

A resistance torque T_R can be obtained by the integral of the shear stress $\tau_x(\theta)$ as follows [3]:

$$T_R = r^2 b \int_{\theta_r}^{\theta_f} \tau_x(\theta) d\theta \tag{8}$$

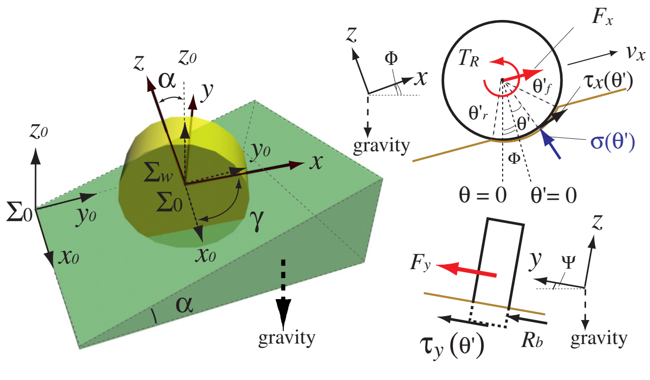

Fig. 3: Definition of the wheel coordinate on inclined surface

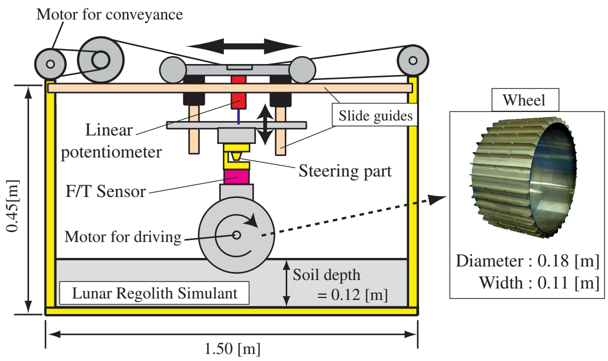

Fig. 4: Schematic view of the single wheel test bed

2.6 Wheel model on inclined surface

We have applied our wheel-soil contact model to an inclined surface as described in Fig. 3. In this case, the definition of the wheel coordinate system $\{\Sigma_w\}$ is considered to be equal to the horizontal case. The inclined surface is assumed to be uniform and a slope angle is denoted by α. When an inertial coordinate system is expressed by $\{\Sigma_0\}$ as a right-hand system, the traverse direction of a slope is denoted by x_0 and the vertical direction by z_0.

The coordinate transformation from $\{\Sigma_0\}$ to $\{\Sigma_w\}$ is employed by a rotation around the x_0 axis with α, then another rotation around the z_0 axis with γ. The angle composed between the planar surface x_0-y_0 and x (or y) axis is determined by Φ (or Ψ).

As shown in Fig. 3, the wheel angle θ' is given by $\theta' = \theta - \Phi$ while θ' is supposed to be zero in the normal direction of the inclined surface. Note that stress distributions of a wheel on an inclined surface are assumed to be equivalent to the case of a horizontal surface and independent to Φ and Ψ.

Using θ' instead of θ, wheel forces on an inclined surface can be derived in the same fashion as equations (6), (7) and (8).

3. Single Wheel Experiment and Simulation

Single wheel experiments are carried out to clarify characteristics of both the drawbar pull and the side force. Also the experimental results are compared to numerical simulation results obtained from the wheel-soil contact model.

3.1 Single wheel test bed

Fig. 4 shows the schematic view of the single wheel test bed. The test bed is constituted by both a conveyance unit and a wheel-driving unit. A steering angle (which is equivalent to a slip angle in this test bed) is set between the conveyance unit and the wheel. Encoders that are mounted at both the conveyance motor and the wheel-driving motor respectively measure a translational velocity and an angular velocity of the wheel. Forces and torques generated by the wheel locomotion are measured by a 6-axis force/torque sensor located between the steering part and the wheel. A wheel sinkage is obtained by the use of a linear potentiometer. The wheel with a diameter of 0.18 [m] and a width of 0.11 [m] is covered with paddles of 0.01 [m] heights. The load of the wheel is 64.7 [N].

In the following experiments, the wheel is controlled to rotate with a constant velocity (= 0.030 [m/s]) by the driving motor mounted inside of the wheel. The translational velocity of the wheel is also controlled so that a slip ratio of the wheel is set from 0.0 to 0.8 with a step of 0.1. The slip ratio is constant during every single run. Also, the value of a slip angle of the wheel is given from 0 [deg] to 30 [deg] with a step 5 [deg].

A vessel of the single wheel test bed is filled up with 12 [cm] of loose soil called "Lunar Regolith Simulant" which simulates the lunar surface soil's material components and mechanical characteristics [1].

Table 1: Simulation parameters and values

parameter	value	unit
c	0.80	[kPa]
ϕ	37.2	[deg]
k_c	1.37×10^3	[N/m^{n+1}]
k_ϕ	8.14×10^5	[N/m^{n+2}]
n	1.00	
k_x	$0.043\times\beta + 0.036$	[m]
k_y	$0.020\times\beta + 0.013$	[m]

3.2 Numerical simulation procedure

The simulations were performed under the same conditions of the single wheel experiments. Parameters used in the simulations are listed in Table 1. The shear deformation modules k_x and k_y are given as functions of a slip angle β. A drawbar pull and a side force of a wheel are calculated by equations (6) and (7), respectively. Also, a resistance torque to a wheel is obtained by equation (8).

3.3 Results and discussion

Experimental measurements of a drawbar pull and a side force are respectively plotted in Fig. 5-(a) and Fig. 5-(b), for each slip angle from 5 [deg] to 30 [deg]. Theoretical curves calculated by the wheel-soil contact model are also drawn in the corresponding figures.

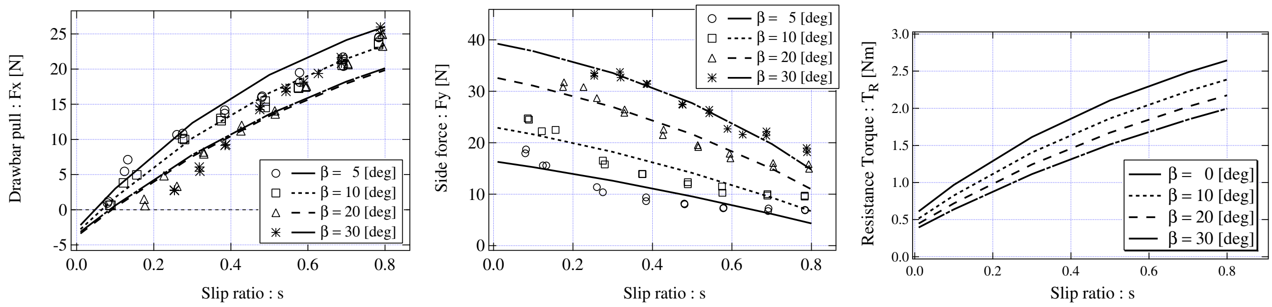

(a) : Slip ratio - Drawbar pull (b) : Slip ratio - Side force (c) : Slip ratio - Resistance torque

Fig. 5: Experimental and simulation results

From Fig. 5-(a), it is seen that the drawbar pull increases as the slip ratio increases, but it decreases as the slip angle increases. Fig. 5-(b) also shows that the side force decreases along with the slip ratio and increases according to the slip angle.

Regarding the resistance torque, it is relatively difficult to directly measure the torque in the experiments. Therefore, we confirm the characteristics of the resistance torque through the numerical simulation. Theoretical curve of the resistance torque is described in Fig. 5-(c). According to the simulation result, the resistance torque increases with an increase in the slip ratio and decreases as the slip angle increases.

4. Slope Travesability Criteria

The criteria determining the slope traversability of the rover are proposed as “mobility limit” and “trafficability limit.” These criteria can be explained by the use of the wheel-soil contact model which we developed as mentioned in Section 2.

4.1 Mobility limit

The mobility limit is discussed based on the relationship between the resistance torque and torque limit of a wheel driving motor. The slip ratio must become larger when a rover travels on an inclined surface. The resistance torque increases along with the slip ratio as already shown in Fig. 5-(c). Then, a wheel driving motor will be suspended if a resistance torque to the wheel is larger than the torque limit of the motor. In a case that one of wheel motors is suspended, resistance torques to the other active wheels must increase and finally all wheel motors will be deactivated. Thus, the mobility limit can be defined as the case when resistance torque T_R equals to or exceeds the torque limit of a wheel motor τ_{limit} as follows:

$$\text{Mobility Limit} \;:\; T_R \geq \tau_{limit}$$

For instance, Fig. 6 describes a theoretical model of the mobility limit. The Motor-A in the figure has a small torque limit, therefore, when a resistance torque exceeds its torque limit at an arbitrary slope angle, the mobility limit can be determined at that slope angle. However, if the wheel equipped the Motor-B having larger torque limit than that of the Motor-A, the resistance torque never overcome the torque limit of the Motor-B even if the slip ratio become 1.0 in which the resistance torque is maximized. Then, the rover can keep traveling and there is no mobility limit in the case of the Motor-B.

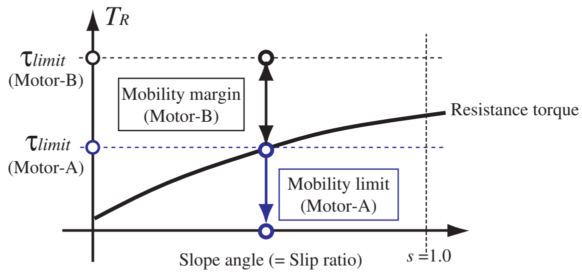

Fig. 6: Mobility limit

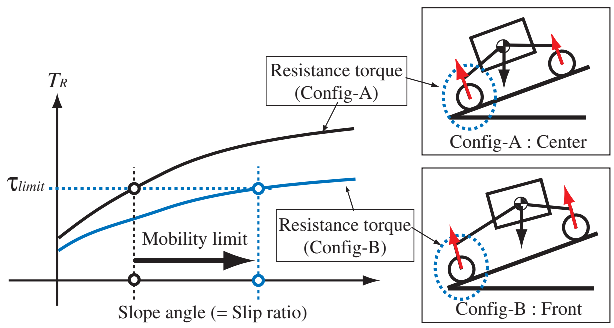

Fig. 7: Improvement of mobility limit

In order to improve the mobility limit, the simplest way is to use a high-torque motor. However, it has to be considered that the high-torque motor will expend more energy of a rover's electric power.

On the other hand, according to the terramechanics theory, resistance torque is originally dependent on a vertical load of each wheel if the slip ratio is constant. Thus, equally dividing the vertical load into each wheel by shifting the centroid of the rover will be also effective to improve the mobility limit. As shown in Fig. 7, it is expected to diminish the resis-

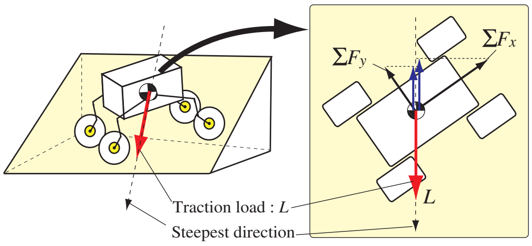

Fig. 8: Trafficability limit

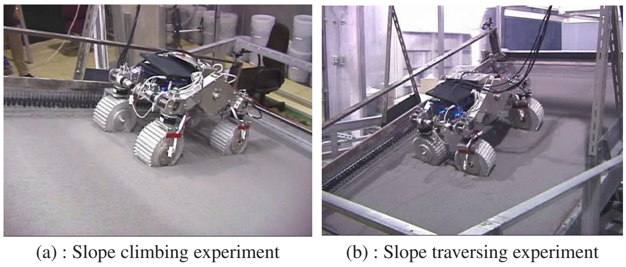

Fig. 9: Slope traversability experiment

tance torque of the rear wheels of the rover by shifting the centroid of the rover ahead from the Config-A to Config-B.

4.2 Trafficability limit

As described in Fig. 8, when the traction load L of a rover is larger than the summation of both components ΣF_x and ΣF_y in the steepest direction, the rover is not able to climb or traverse the slope even if each wheel driving motor has enough torque to avoid the mobility limit. Here, ΣF_x is a summation of the drawbar pulls of all the wheels, whereas ΣF_y means that of the side forces. Thus, the trafficability limit can be defined when a traction load of a rover L equals to or overcomes a traction force $|\overrightarrow{\Sigma F_x} + \overrightarrow{\Sigma F_y}|$ of the rover as follows:

$$\text{Trafficability Limit} \ : \ L \geq \left| \overrightarrow{\Sigma F_x} + \overrightarrow{\Sigma F_y} \right|$$

The trafficability limit is simply enhanced by increasing those traction forces. As mentioned in Fig. 5-(a), the drawbar pull has a maximum value at $s = 1.0$, however a rover at $s = 1.0$ is not able to travel anymore. In addition, a wheel with high slip causes soil destruction around the wheel. It is therefore needed to control each wheel to drive with an appropriate slip where the slip-traction effectiveness (=drawbar pull/slip ratio) takes the maximum value.

Regarding the side force, the larger the slip angle is, the larger the side force becomes. If the steering angle of each wheel is properly given, a rover will traverse a slope. However in the case that a slope is covered with loose soil, the soil at the side face of the wheel moves down the slope as in a snow avalanche when the wheel has a large enough side force to overcome the bearing stress of the soil. Hence, according to the above discussions, the trafficability limit is redefined as a limit of the soil bearing capacity.

5. Slope Traversability Experiments

The slope experiments were conducted using our rover test bed in order to analyze the slope traversability. The experiments are divided into slope climbing and slope traversing experiments.

5.1 Experimental setup

Fig. 9 shows overviews of the experimental setup with our rover test bed. The facility located at Japan Aerospace Exploration Agency (JAXA) consists of a flat rectangular vessel in the size of 1.5 by 2.0 [m] filled up with 10 [cm] depth of the Lunar Regolith Simulant. The vessel can be inclined up to 30 [deg].

The four-wheeled rover test bed developed by the author's group has a dimension of 0.62 [m](length) × 0.53 [m](width) × 0.46 [m](height) and weights about 35 [kg] in total. Each wheel of the rover is the same as the wheel used in the single wheel experiment. All wheels have an active steering axle.

During the experiments, the rover test bed travels with a given angular velocity and a steering angle. Each wheel is controlled to travel with a constant angular velocity as 12 [rpm] and an arbitrary steering angle by an on-board computer. We measured a motion trajectory of the rover using 3D optical sensors. Force/torque sensors are mounted on upper part of each wheel to measure the forces generated by the corresponding wheel.

Table 2: Slope climbing experiment

Motor	Configuration	Max slope angle : (Criteria)
Motor-A	Config-A	14 [deg] : (Mobility limit)
Motor-A	Config-B	19 [deg] : (Mobility limit)
Motor-B	Config-A	21 [deg] : (Trafficability limit)
Motor-B	Config-B	21 [deg] : (Trafficability limit)

5.2 Slope climbing experiment and discussion

In the slope climbing experiment, the slope angle is given from 10 [deg] to the angle which the rover cannot climb up. The wheel driving motors are chosen to have two different types of torque limits (Motor-A=2.0 [Nm]/ Motor-B=10.0 [Nm]) to discuss the mobility limit. Also, the configurations of the rover are given two different centroid positions as the Config-A (center) and Config-B (front) as shown in Fig. 7.

The experimental results are summarized in Table 2. Through a number of the climbing experiments, the maximum slope angle for the slope climbing using the Motor-A was 14 [deg] because the motor was suspended. This result indicates that the resistance torque to the wheel might exceed the motor torque limit, and this was the mobility limit. On the other hand, the maximum slope angle using the Motor-B is 21 [deg] since the slip ratio of each wheel is almost 1.0 but the wheel is not suspended. The soil destructions around the driving wheel were observed in that slope

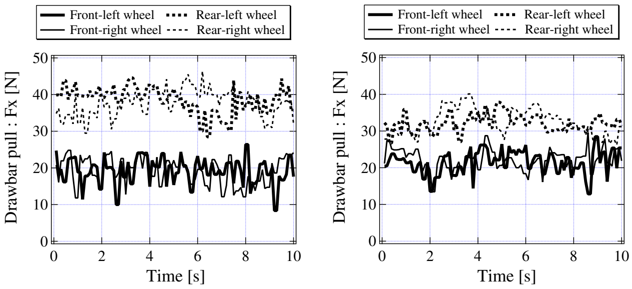

(a) : Config-A (b) : Config-B

Fig. 10: Time profile of drawbar pull

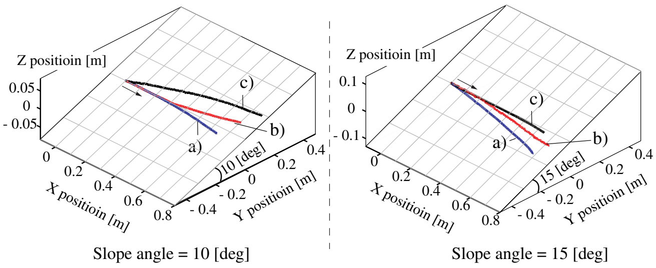

Fig. 11 : Slope traversing experiments (a) no steering, b) each of front wheels has 15 [deg], c) every wheel has 15 [deg].)

angle. The trafficability limit gives this result as 21 [deg] for the maximum slope angle.

In the case of using the Motor-A, we found that the maximum slope angle with Config-B was improved to 19 [deg], while without shifting the centroid of the rover (Config-A) it was able to climb up to only a slope of 14 [deg]. This result indicates that the resistance torque was successfully diminished by shifting the centroid of the rover ahead.

It must be emphasized that the effectiveness by shifting the centroid of the rover was not seen in the case of using Motor-B. This reason is deduced because the summation of the drawbar pulls of all wheels is almost the same value even in both cases. In fact, in the case a slope angle of 21 [deg], the traction load of the rover L was 115 [N] and the summation of the drawbar pulls was about 110 $\sim$ 120 [N] in both rover configurations as shown in Fig. 10.

5.3 Slope traversing experiment and discussion

We also conducted the slope traversing experiment using the Motor-B. In the experiment, the rover is given three different steering configurations; a) no steering, b) steer only front wheels with a steering angle of 15 [deg], and c) steer all wheels with a steering angle of 15 [deg].

According to the experimental result as shown in Fig. 11, it is clearly seen that the larger the slope angle becomes, the more significant a skid motion of the rover is. Additionally, the rover is not able to climb and traverse a slope angle of 15 [deg] with any steering configurations. The summation of the drawbar pulls and the side force must be smaller than the traction load of the rover. Thus, the slope angle of 15 [deg] is the trafficability limit in the cases of those steering configurations.

6. Conlusion

This paper described the slope traversability analysis based on the terramechanics. The criteria dominating the slope traversability are elaborated and validated along with the single wheel experiments and the slope climbing/traversing experiments. The proposed criteria can be concluded that the mobility limit depends on a vehicle performance (e.g. motor torque and vehicle configuration), whereas the trafficability limit is determined by a wheel-and-soil interaction (soil destruction around wheel.)

Based on the mobility limit, we can conclude what kinds of motors are appropriate in an actual mission. Moreover, using the trafficability limit, we can find a better control algorithm to climb/traverse a slope and avoid a large slip/skid motion which may cause mission failures such as a stuck rover or a tipover.

References

[1] Heiken, G., Vaniman, D., French, B. M., and Schmitt, J., "Lunar Sourcebook : A User's Guide to the Moon," Cambridge University Press, 1991.

[2] Bekker, M. G., "Off-The-Road Locomotion," The University of Michigan Press, 1960.

[3] Bekker, M. G., "Introduction to Terrain-Vehicle Systems," The University of Michigan Press, 1969.

[4] Wong, J. Y., "Theory of Ground Vehicles," John Wiley & Sons, 1978.

[5] Iagnemma, K., Shibly, H., and Dubowsky, S., "On-Line Traction Parameter Estimation for Planetary Rovers," Proc. of the 2002 IEEE Int. Conf. on Robotics and Automation, pp. 3142–3147, 2002.

[6] Iagnemma, K. and Dubowsky, S., "Mobile Robot in Rough Terrain," Springer Tracts in Advanced Robotics, vol.12, 2004.

[7] Yoshida, K., Mizuno, N., Ishigami, G., and Miwa, A., "Terramechanics-Based Analysis for Slope Climbing Capability of a Lunar/Planetary Rover," 24th Int. Symp. on Space Technology and Science, 2004-k-06 2004.

[8] Ishigami, G. and Yoshida, K., "Steering Characteristics of an Exploration Rover on Loose Soil Based on All-Wheel Dynamics Model," Proc of the 2005 IEEE Int. Conf. on Intelligent Robots and Systems, pp. 2041-2046, 2005.

[9] Wong, J. Y. and Reece, A. R., "Prediction of Rigid Wheel Prefoemance Based on the Analysis of Soil-Wheel Stresses Part I, Preformance of Driven Rigid Wheels," Journal of Terramechanics, vol.4, 1967.